An optical gas imaging technique based on strobed illumination

Mathews Chirindo[1], *Ettienne* Cox[2], *Kahesh* Duness[1]

[1]Council for Scientific and Industrial Research, Manufacturing Cluster, Pretoria, South Africa

[2]Council for Scientific and Industrial Research, Defence and Security Cluster, Pretoria, South Africa

Abstract. Gas leakage from equipment poses undesirable safety, environmental and operational impacts. Many optimal gas imaging techniques exist which detect and visualize gas plumes. However, most of these techniques struggle to produce clear images when the temperature gradient between the scene background and the gas plume is small. This paper presents an optical gas imaging technique that is based on strobed illumination, wherein the strobing frequency of the illuminating device is associated with the camera frame rate. Experimental test results are presented to show the improved detection of volatile organic compound gases during strobed illumination under dark room laboratory conditions where the percentage contrast value of the illuminated gas relative to its background varies by 50.8% The test results for the detection of sulphur hexafluoride gas and liquid petroleum gas under an outside environment are also presented.

1 Introduction

The leakage of gas from pipelines and other equipment has a significant undesirable impact on the safety, environmental and operational requirements. Most countries worldwide impose tough legislation that restricts spillage of and pollution due to hazardous and greenhouse gases. In most cases, these gases are odourless and invisible to a naked eye and may cause harm unnoticed. Gases of particular concern in the context of this paper are sulphur hexafluoride (SF6) and Volatile Organic Compounds (VOC).

SF6 gas is widely used in Insulated Gas Switchgear (GIS) equipment because of its excellent insulation and arc extinguishing properties [1]. The operation of GIS equipment may be accompanied by SF6 gas leakage which could decrease the insulation performance of equipment [2]. Moreover, the decomposition of the SF6 gas produces by-products which are severely corrosive and toxic. VOCs are organic chemical compounds which can vaporise easily at room temperatures. Some of their main sources of emission include the petrochemical, agriculture, energy and waste sectors [3]. VOCs are highly flammable and toxic leading to explosions and/or dangers to health if they are left undetected. In view of this background, it is of paramount importance that SF6 and VOC gas leaks from different sources be detected early, before a catastrophic danger is experienced.

Many gas detection methods have been developed over time. Such methods include carbon nanotube sensor detection [4], differential absorption lidar detection [5], photoacoustic spectroscopy detection [6] and acoustic signal detection [7], [8] for SF6 detection. However, these methods/techniques lack imaging capabilities which are essential for gas visualization [1]. Reference [9] reports an interesting method for methane gas detection and quantification using remote sensing and sensor data fusion. However, this method is relevant for experimental work in the laboratory and might be difficult to implement in field applications.

Many optimal passive and/or active gas imaging techniques to detect and visualize gas plumes exist. Reference [1] reports intelligent gas leakage detection in confined spaces based on image recognition and claims superior gas detection accuracy against other mainstream imaging methods [2], [10] in the presence of background heat disturbances. The techniques described in [1] and [2] present tedious offline training processes of the convolutional neural network algorithms that entails huge computational requirements.

This paper presents a simple and improved optical gas imaging technique that is based on strobed illumination wherein the strobing frequency of the illuminating device is associated with the camera frame rate. The technique is presented to show the improved detection of volatile organic compound gases in dark room conditions, particularly when the temperature difference between the gas and the background is small.

The rest of the paper is organized as follows: Section 2 provides some background on electromagnetic absorption spectrum. Section 3 presents the development of the detection technique – methodology. Section 4 describes the experimental setup while Section 5 presents and discusses the experimental test results. Section 6 concludes the paper. Section 7 is the acknowledgment.

2 Theoretical background

Most gas leak detectors are based on infrared spectroscopy and depend on the property of gases to absorb the infrared energy at specific wavelengths. As depicted in Fig.1, the infrared band falls in the electromagnetic spectrum after the visible band. It is further divided into sub-bands as shown. Different gases have certain absorption characteristics based on their position in the sub-bands of the infrared spectrum, for example SF6 gas lies in the Medium Wave Infrared (MWIR) sub-band while VOC gases lie in the Long Wave Infrared sub-band (LWIR).
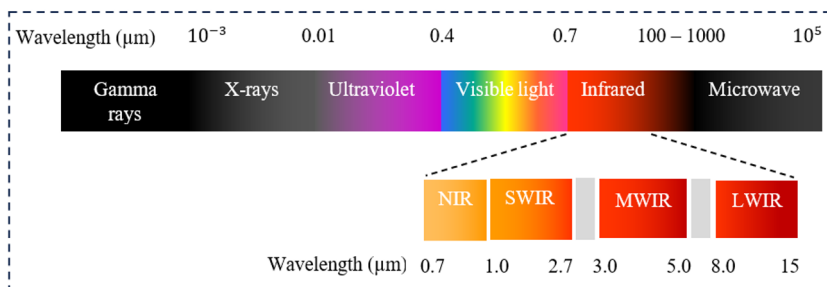

Fig.1. Position of the infrared band in the electromagnetic spectrum.

When gas absorbs infrared energy, its temperature increases, and it starts to radiate heat based on its absorption characteristic in the infrared spectrum. The radiation intensity, I_t transmitted by a gas (neglecting scattering and assuming constant absorption coefficient, α_λ) at temperature, T and wavelength, λ is given by Lambert-Beer law [9]:

$$I_t(T, \lambda) = I_o(T, \lambda) . e^{-\alpha_\lambda . \bar{C} . l} \qquad (1)$$

where, I_o is the incident radiation that passes through the gas while $\bar{C}$ and l are the irradiated volume and the pathlength the irradiated gas passes through, respectively.

When passive gas leak detection is employed, the source of incident radiation is the scene background. Passive infrared gas leak detection sensors are cheaper and are lower powered compared to active infrared sensors. The detection, visualization and location of gas leaks using passive infrared sensors is performed in a relatively easy way. However, passive infrared detection struggles to perform when the temperature difference between the gas and the background is small.

When active gas leak detection is employed, the source of incident radiation is an artificial source e.g. laser source. The goal is to illuminate the gas with artificial energy so that its temperature differs from that of its environment by a recognizable margin. Under these circumstances it is easier to selectively detect the gases and present clearer images since the system attains higher sensitivity.

The technique presented in this paper employs a passive infrared detector for gas visualization and active gas illumination to improve visibility when the temperature gradient of the gas and its background scene is small. Moreover, it detects more than one type of gas, rendering its applicability in different industrial environments e.g. electrical power, petro-chemical industries etc.

3 Development of gas imaging technique

3.1 Strobed illumination

The developed strobed illumination structure consists of the strobing wheel, the infrared
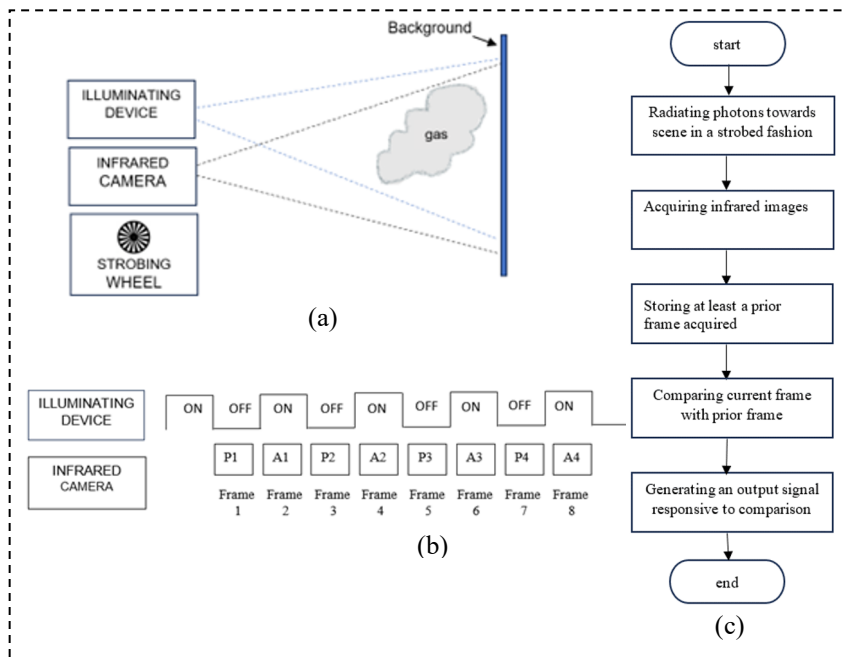

Fig. 2. Illustrating strobed illumination [11] (a) the concept (c) the mechanism (c) the flowchart.

camera front optics and the illuminating device as shown in Fig. 2(a). The strobing wheel is a perforated disc that is physically placed in front of the illuminating device. It is driven by software at a speed that is comparable to the camera frame rate. It operates on the principle of stroboscopic effect that causes rotating objects to appear still when represented by a series of short samples at a sampling rate close to the period of rotational motion. The infrared front optics consists of the lens for field of view adjustment, the filter with specific gas spectral response and the infrared detector. The illuminating device is a tungsten or halogen lamp that illuminates the gas (and the background) to increase the signal to noise ratio (or gas contrast) in the LWIR and MWIR bands. The strobing mechanism is shown in Fig. 2(b) where the illuminating device is strobed between ON and OFF by the strobing wheel. It would radiate photons at a specific gas absorption wavelength during an ON-state and would not radiate photons during an OFF-state. The infrared camera, therefore, alternately captures active and passive frames at a maximum frame rate of 60 Hz. The flowchart for the strobed illumination and the capturing of images is shown in Fig. 2(c).

3.2 Optical gas image processing

3.2.1 Image processing system

The development of the optical gas image processing system presented in this paper uses GasCAM which is a commercial system that has direct application in industry for the detection and visualization of gas leaks. Fig. 3 shows the image processing system which consists of hardware and software components that interface with user buttons for manual control input and LCD device for video monitoring. The input/output interface connects to various supporting modules including controls for power up and power down sequencing as well as support for video recording and playback. The laser pointer assists in aiming, targeting or locating the scene of interest. The visible camera is included as a baseline indicator of the scene.
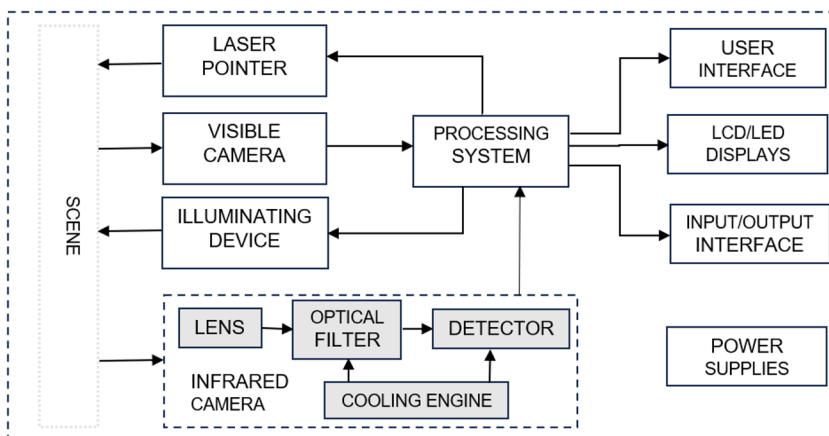

Fig. 3. Overview of the optical gas imaging system.

3.2.2 IR image processing

The infrared image processing block diagram is shown in Fig. 4. The infrared image signal from optical frontend and Irnova320ER ICDA cooled detector is first pre-processed by concatenating two 8-bit data per pixel into one 16-bit data per pixel. The resulting image

signal is passed to a one-time or on-demand Non-Uniformity Correction (NUC) to compensate for the differences in gain and offset between individual pixels in the raw data. Each corrected image frame, $F_{corrected}$ is obtained from [12]:

$$F_{corrected} = F_{raw} * Gain + Offset \qquad (2)$$

where F_{raw} is the raw image frame. The Gain and Offset values are calculated from equations (3) and (4) respectively. In this case, two reference images are required at two different scene temperatures. A series of 16 images is captured at each of the two reference temperatures to eliminate temporal noise, and then a temporal median, $median(T_{high})$ or $median(T_{low})$ of each pixel is calculated to represent the pixel value in the reference images. The gain and offset values are then calculated as follows:

$$Gain = \frac{median(T_{high}) - median(T_{low})}{T_{high} - T_{low}} \qquad (3)$$

$$Offset = T_{low} - G.T_{low} \qquad (4)$$

where T_{high} and T_{low} are the reference temperature values at high temperature and low temperature respectively.

The temperature of the scene does not normally cover the entire detectable temperature range of the infrared camera. Therefore, it is necessary to set the upper and lower temperature limits of the scene of interest. This is achieved by the span and level settings in the image processing chain. The span can be used to set the uppermost temperature range value for the displayed image above the level while the level sets the lowermost bound temperature for the displayed image. On the other hand, a subtraction operation can be selected to detect moving
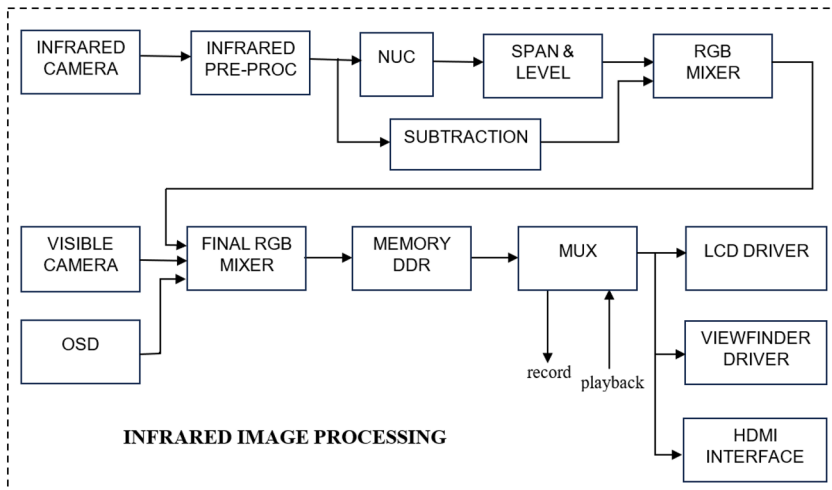

Fig. 4. Infrared image processing block diagram.

objects only, for instance, flowing gas. This is achieved by comparing the current frame and the prior frame and subtracting the same from each other. The prior frame can either be active or passive frame. This operation cancels out all stationary objects in the scene.

The visual image and On-Screen Display (OSD) information is included in the final RGB mixer stage before the information of interest is sent to the LCD display, viewfinder display and to the external HDMI interface. The images can be recorded on or played back from disk.

4 Experimental setup

The experimental results presented in section 5 were captured from two separate setups, an indoor dark room laboratory (Fig. 5) and an outdoor gas leak test. In the indoor dark room laboratory setup (results shown in Fig. 6 to Fig. 8) the experiments were carried out to
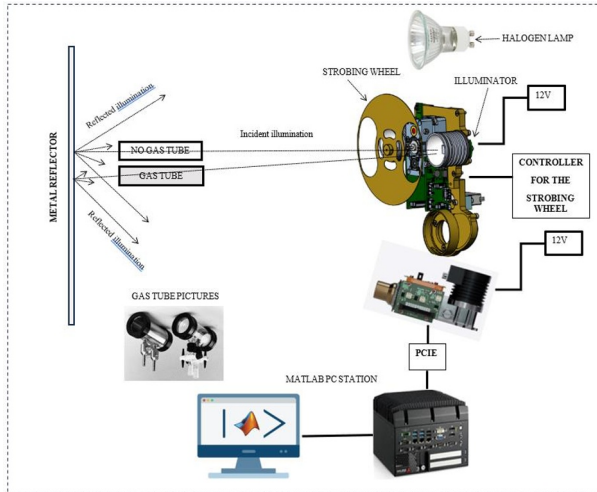

Fig. 5. Experimental setup.

demonstrate the effect of strobed illumination on gas visibility. The image processing was performed using the image processing tools in the MATLAB environment. The illumination was provided first by a laser and then by a tungsten and/or halogen lamp. The strobing wheel was assembled to interrupt the light/heat path at the strobing frequency determined by the controller, wherein the strobed light/heat passes through the gas tubes, one with LPG gas and other with no gas. The reflected light/heat from the metal detector is received by the IRNOVA320ER cooled infrared detector. The output image of the infrared detector is routed via the PCIE interface to a MATLAB PC for processing.

In the outdoor gas leak setup, the results were captured using the GasCAM product which was developed using the concept of Fig. 5. Gas leaks were simulated using an SF6 gas bottle in the outside environment.

5 Experimental results

To verify the effectiveness of the optical gas imaging technique, the results of the experimental tests are presented. Fig. 6 illustrates the effect of laser strobing on gas visibility. The strobing frequency must be comparable to the infrared camera frame rate while the strobed light must emit photons in the gas absorption spectrum. It is seen that laser light strobing has the effect of improving the visibility of gas particularly when a subtraction of the frames grabbed during no strobing and those grabbed during strobing is performed. The pixel intensity on the gas tube is less (darker) than on the reference tube in the subtracted result due to the gas spectral absorption. Assuming the pixel intensities in the reference cell to be representative of the background, it is found that the percentage contrast value, c of the illuminated gas relative to its background varies by 50.8% based on the following:

$$c(\%) = \frac{|\bar{P}_g|}{|\bar{P}_r|} \times 100 \qquad (5)$$
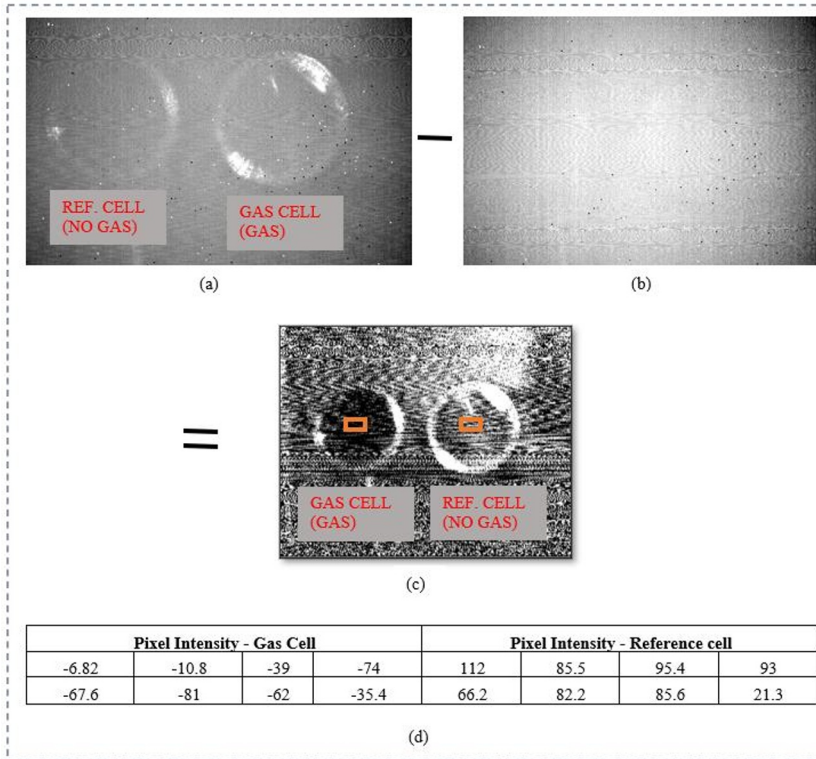
Pixel Intensity - Gas Cell				Pixel Intensity - Reference cell			
-6.82	-10.8	-39	-74	112	85.5	95.4	93
-67.6	-81	-62	-35.4	66.2	82.2	85.6	21.3

(d)

Fig. 6. Illustration of the laser strobing effect on gas visibility (a) laser strobing (b) no strobing (c) subtraction of (a) and (b) (d) pixel intensity values.

where $\bar{P}_g$ and $\bar{P}_r$ are the mean pixel values for the gas cell and reference cell samples respectively.

The effect of the halogen lamp strobed illumination on the gas cell when compared with the reference cell is shown in Fig. 7. The gas is more visible in the gas cell than in the reference cell during strobed illumination.

Illumination can either be strobed or continuous. The effect of continuous illumination is shown in Fig. 8. It also results in visibility of the gas. However, continuous illumination is theoretically less powerful than strobed illumination particularly in the presence of strong ambient lightning, etc.
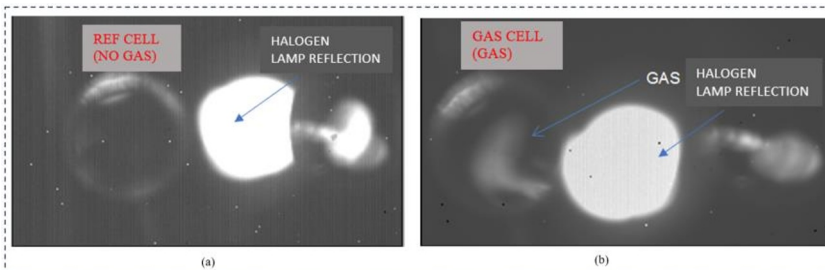

Fig. 7. Effect of halogen lamp strobed illumination on gas visibility (a) reference cell (b) gas cell.
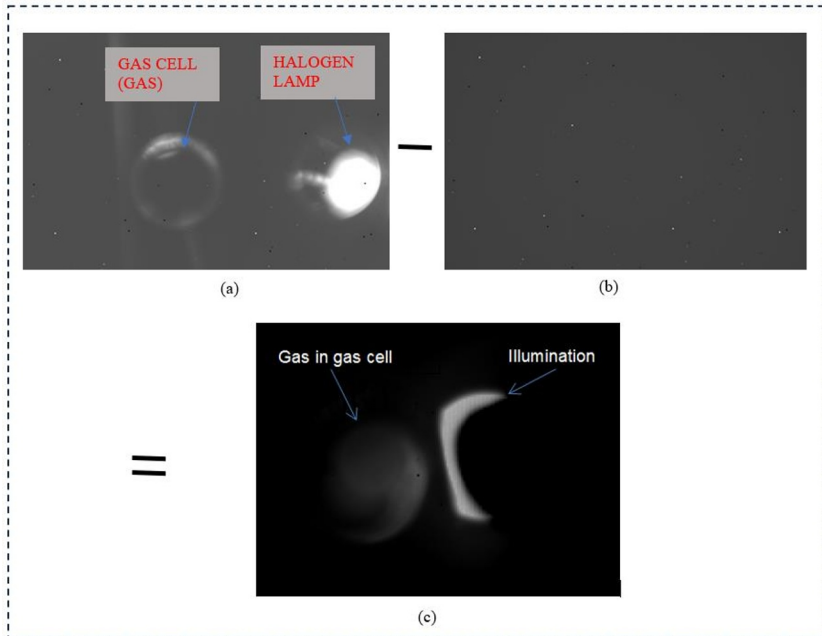
Fig. 8. Effect of continuous illumination on gas visibility (a) illumination on (b) illumination off (c) illuminated gas.

Fig. 9 shows the fundamental test results for the detection of SF6 and VOC gases e.g. LPG gas. It is seen that the respective gases are clearly visible, thus demonstrating the effectiveness of the developed infrared gas detection camera under natural environmental conditions. The severity of gas leaks can vary in different field circumstances. In Fig. 10, the detection of small, medium and large leaks is demonstrated. The high sensitivity of the gas detection camera enables it to detect very small leaks in pipelines or gas insulated switchgear installations.

Fig. 9. Optical gas detection (a) SF6 gas detection (b) VOC - LPG gas detection.
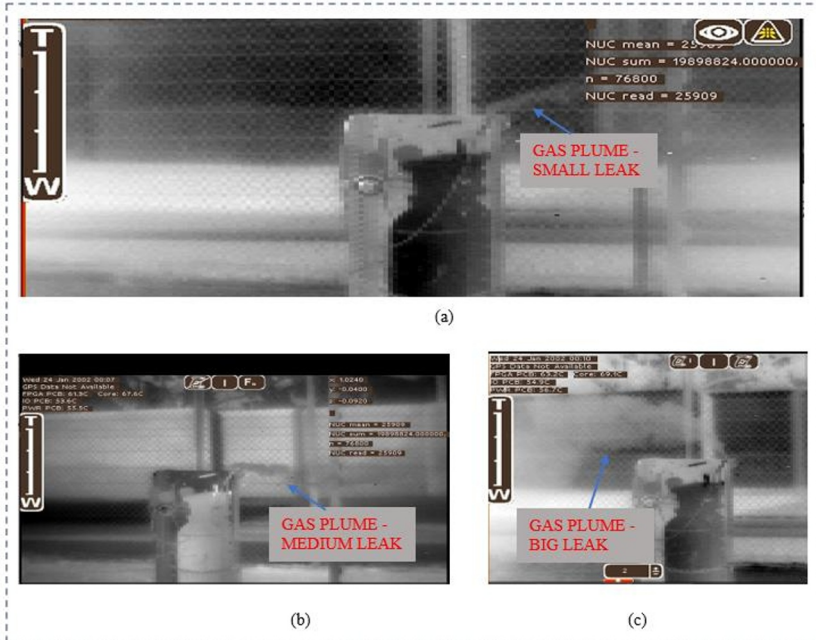
Fig. 10. Sulphur hexafluoride leak detection (a) small leak (b) medium (c) big leak.

6 Conclusion

An optical gas imaging methodology based on strobed illumination has been presented in the paper. Experimental results have shown improved gas visibility of the subtracted image during strobed illumination where the percentage contrast value of the illuminated gas relative to its background varies by 50.8%. It is also evident that continuous illumination results in gas visibility when compared to no illumination. The fundamental test results for the detection of SF6 and LPG gas leaks is further presented. It is shown that the developed gas detection camera can detect leaks of varying severity ranging from small to large leaks owing to its high sensitivity. The gas detection camera can detect both SF6 and VOC gas leaks as applicable to electrical power and petro-chemical industries.

However, based on the presented test results, it is recommended that further tests be conducted as part of future research to demonstrate the effect of strobed illumination on flowing (rather than static) gas.

References

1. J. Huang, B. Chen, S. Chen, G. Xiao, J. Yan and Z. Wang, "Research on Intelligent Detection of Sulfur Hexafluoride Gas Leakage in Confined Spaces," *2022 6th International Conference on Electric Power Equipment - Switching Technology*

ICEPE-ST, Seoul, Korea, Republic of, pp. 18-22, (2022), doi: 10.1109/ICEPE-ST51904.2022.9757072

2. K. Xu, Z. Yuan, J. Zhang, Y. Ji, X. He and H. Yang, "SF6 Gas Infrared Thermal Imaging Leakage Detection Based on Faster-RCNN," *2019 International Conference on Smart Grid and Electrical Automation, ICSGEA*, Xiangtan, China, pp. 36-40, (2019), doi: 10.1109/ICSGEA.2019.00017.

3. I. Karakurt, G. Aydin and K. Aydiner, "Sources and mitigation of methane emissions by sectors: A critical review," *Renewable Energy*, 39(1), pp. 40-48, (2012).

4. X. Zhang, W. Liu, J. Tang, and F. Meng, "Experimental study on the detection of SF6 discharge decomposition components by carbon nanotube sensors," *Electrical Engineering magazine*, 26(11), pp. 121-126, (2011).

5. H. Kariminezhad, P. Parvin, F. Borna, and A. Bavali, "SF6 leak detection of high-voltage installations using TEA-CO2 laser-based DIAL," *Optics and Lasers in Engineering*, 48(4), pp. 491-499, (2010).

6. K. Li, F. Ma, H. Zhu, F. Zhu, and D. Han, "Effect of SF6 content on detection sensitivity in SF6/N2 fault decomposition gas detection based on photoacoustic spectroscopy," *Electrical Engineering magazine*, 35(17), pp. 3773-3780, (2020).

7. A. Sampaolo, P. Patimisco, M. Giglio, L. Chieco, G. Scamarcio, F. K. Tittel, and V. Spagnolo, "Highly sensitive gas leak detector based on a quartz-enhanced photoacoustic SF6 sensor," *Optics Express*, 24(14), pp. 15872-15881, 2016.

8. Y. Yang, "Design of an Multi-sensor Ultrasonic Detection System for SF6 Gas Leak in Power System," *2020 IEEE 4th Conference on Energy Internet and Energy System Integration, EI2*, Wuhan, China, pp. 3935-3939, (2020), doi: 10.1109/EI250167.2020.9347155.

9. S. Dierks and A. Kroll, "Quantification of methane gas leakages using remote sensing and sensor data fusion," *2017 IEEE Sensors Applications Symposium, SAS*, Glassboro, NJ, USA, pp. 1-6, (2017), doi: 10.1109/SAS.2017.7894047.

10. Q. Lu, Q. Li, L. Hu, and L. Huang, "An Effective Low-Contrast SF_6 Gas Leakage Detection Method for Infrared Imaging," *IEEE Transactions on Instrumentation and Measurement*, 70, pp. 1-9, (2021), doi: 10.1109/TIM.2021.3073443.

11. E. Cox, "A gas detection system and method, United States Patent US 20200363327A1," Nov. 19, (2020).

12. A.B.G., "Operating the IRnova320ER IDCA series," IRnova A.B., Kista, Sweden, Rep. irn053180.